

S2M-Trek: From Single to Multi-Sphere Transport via Per-Frame Deep Sets on a Wheel-Legged Robot

Zong Chen^{1,†} Xuebin Li² Jinpeng Xiao¹ Shaoyang Li¹
Ben Liu¹ Min Li¹ Zhouping Yin¹ Yiqun Li^{1,*}

¹School of Mechanical Science and Engineering, Huazhong University of Science and Technology

²School of Mathematics, Harbin Institute of Technology

*Corresponding author †skelton_chan@hust.edu.cn

Abstract: We study the problem of scaling dynamic loco-manipulation from a single free-rolling sphere to multiple spheres transported simultaneously on the back of a wheel-legged quadruped, without fences, grippers, or mechanical stops. Multiple identical free-rolling spheres form an unordered set with no persistent identity: their ordering may change independently at each history frame, creating a *per-frame permutation symmetry* that standard history-concatenation set encoders do not explicitly enforce—these encoders impose only a shared, diagonal permutation symmetry over the full history. We show that this symmetry mismatch leads to a concrete failure mode in curriculum-based reinforcement learning. Within the same PPO training budget, flat MLPs and branch-wise encoders plateau at or below the two-sphere stage, while a history-concatenation Deep Sets baseline (DSHC) fails to progress past the two-sphere stage in our runs unless ball-to-slot assignments are randomised during training, suggesting that it exploits slot indices as a curriculum shortcut rather than learning identity-free multi-sphere dynamics. We propose **Per-Frame Deep Sets (PFDS)**, which performs permutation-invariant pooling within each history frame before temporal readout; we prove that PFDS is G_{frame} -invariant and universally approximates continuous G_{frame} -invariant policies. A 2×2 ablation over encoder architecture and slot randomisation separates the architectural and data-augmentation pathways, and PFDS reaches the five-sphere stage with 100% no-drop transport in simulation across all five random seeds. We further distill the PFDS teacher into TACTSET via DAGger, replacing privileged sphere-state observations with a 16×16 Boolean union contact map, yielding a compact and naturally G_{frame} -invariant tactile representation.

Keywords: locomotion, loco-manipulation, permutation invariance, deep sets, teacher-student learning, tactile sensing, multi-object manipulation

1 Introduction

Wheel-legged and legged robots have achieved remarkable locomotion versatility [2, 3, 4, 5], and recent work has extended these platforms to single-object loco-manipulation [6, 7, 8, 9]. Scaling from one object to many, however, is not a simple matter of adding more input channels. Transporting *multiple* free-rolling objects simultaneously—without fences, clamps, or fixed identity labels—changes the representational problem: the objects form an unordered, identity-free set whose slot assignments may change independently from one history frame to the next, a symmetry that prior work has not formalised. This paper studies the problem entirely in simulation; real-robot deployment of the tactile student is in progress and will be reported separately.

This work was supported by the Fundamental and Interdisciplinary Disciplines Breakthrough Plan of the Ministry of Education of China (JYB2025XDXM208).

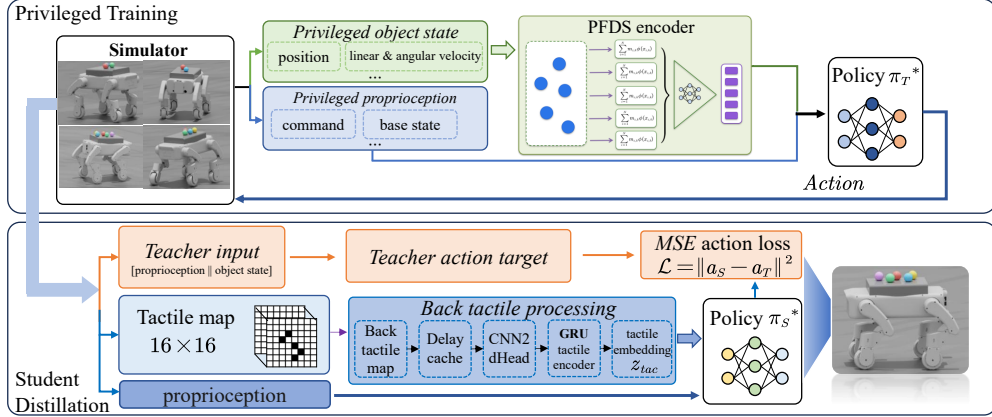


Figure 1: System overview of S2M-Trek (**top**: privileged teacher training; **bottom**: tactile-student distillation pipeline). The PFDS teacher is trained in Isaac Lab [1] with PPO using privileged object-state observations (position, linear/angular velocity). TACTSET is distilled via DAgger, replacing the privileged observation with a 16×16 Boolean union tactile contact map; physical deployment on the robot is in progress and outside the scope of this paper.

The symmetry mismatch problem. Consider the multi-sphere observation tensor $X \in \mathbb{R}^{H \times N \times d}$, where H is the history length, N the maximum number of object slots, and d the per-object feature dimension. Because the spheres are identical, swapping two balls’ slot assignments in any single history frame produces a physically equivalent state. The correct quotient group is therefore the *per-frame* product group

$$G_{\text{frame}} = (\mathfrak{S}_N)^H, \quad (g \cdot X)_{t,i} = x_{t,\pi_t^{-1}(i)}, \quad g = (\pi_1, \dots, \pi_H), \quad (1)$$

not the *diagonal* subgroup $G_{\text{diag}} = \{(\pi, \dots, \pi) : \pi \in \mathfrak{S}_N\} \subsetneq G_{\text{frame}}$ that history-concatenation encoders [10, 11] actually satisfy. The quotient ratio $|G_{\text{frame}}|/|G_{\text{diag}}| = (N!)^{H-1}$ reaches $\approx 1.7 \times 10^6$ for $N=5, H=4$: six orders of magnitude of redundant non-physical variation that G_{diag} encoders cannot collapse.

Two paths to G_{frame} robustness. One can approach G_{frame} invariance in two ways:

1. **Architectural (intrinsic):** Design the encoder so that $f(g \cdot X) = f(X)$ for all $g \in G_{\text{frame}}$ by construction.
2. **Data-augmentation (learned):** Keep a G_{diag} encoder but sample a fresh per-frame slot permutation π_t at every simulation step, implicitly averaging the loss over the G_{frame} orbit.

We show experimentally that these two paths are not interchangeable: the architectural path advances the curriculum in both training regimes, while the data-augmentation path fails to advance past the two-sphere stage when augmentation is absent.

Contributions.

1. We formalise multi-sphere transport as a G_{frame} -invariant policy learning problem, deriving the quotient ratio $(N!)^{H-1}$ as a quantitative measure of the representational gap left unaddressed by standard encoders.
2. We propose **PFDS** (Per-Frame Deep Sets): a minimal modification of standard Deep Sets that achieves G_{frame} -invariance by performing frame-wise pooling before temporal readout, backed by proofs of invariance and universal approximation.
3. We present an eight-encoder comparison and a 2×2 ablation (encoder $\in \{\text{PFDS}, \text{DSHC}\} \times$ augmentation $\in \{\text{on}, \text{off}\}$) that separates the architectural and data-augmentation contributions, and we further confirm PFDS’s reliability across five random seeds.

4. We propose TACTSET, a DAgger-distilled student that replaces privileged ball-state observations with a 16×16 Boolean union contact map—a representation that is *naturally* G_{frame} -invariant—achieving 75% no-drop transport of five spheres in simulation.

2 Related Work

Legged loco-manipulation. Rapid motor adaptation [5] and massively parallel RL [3] laid the foundation for agile locomotion. DribbleBot [6] and follow-up work [7, 8] extended quadrupeds to single-object manipulation, and LocoTouch [9] added back-mounted tactile sensing for cargo transport. To our knowledge, no prior work addresses unconstrained multi-sphere transport or identifies per-frame permutation symmetry as a representational bottleneck for scaling loco-manipulation.

Permutation-invariant networks. Deep Sets [10] introduced the $\rho(\sum_i \phi(x_i))$ universal approximator; Set Transformer [11] and PointNet [12] extended it with attention and point-cloud structure, and Maron *et al.* [13] analysed higher-order tensor invariance. These methods all target *single-frame* sets. We address the strictly harder *multi-frame* case, where each history frame may be permuted independently—a product group $(N!)^{H-1}$ larger than the diagonal group these encoders satisfy.

Equivariant RL and multi-object symmetry. MDP homomorphic networks [14, 15], SE(3)-equivariant manipulation [16, 17], and multi-agent symmetry methods [18] exploit spatial or agent-level structure for sample-efficient RL. None considers the temporal product symmetry arising when identical objects are observed over multiple history frames with independent slot re-assignments.

Tactile sensing and distillation. Tactile sensors support contact-rich manipulation and load transport on legged platforms [19, 20, 21, 22, 9], and DAgger [23] distillation bridges privileged training observations and deployment-feasible sensors. A central obstacle in multi-object settings is that object-indexed teacher representations do not map cleanly to tactile signals; we observe that the Boolean *union* of contact footprints is G_{frame} -invariant by construction and therefore aligns student and teacher representations without explicit permutation bookkeeping.

3 Problem Formulation

Multi-sphere transport MDP. A four-wheel-independent-steering quadruped—self-designed for this study—transports $k \in \{1, \dots, N\}$ identical free-rolling spheres (radius 55 mm) on a flat back plate ($22.4 \text{ cm} \times 15.1 \text{ cm}$). $N = 5$; the robot has 12 leg joints and 4 hub motors, controlled at 50 Hz. A back plate equipped with a 16×16 binary tactile array (256 cells) provides contact feedback. The episode terminates when any ball falls off the plate or the robot falls. Object count k is increased by a multi-criterion curriculum (episode-length ratio, support margin, dangerous fraction, edge-overflow fraction, velocity tracking error).

Multi-ball observation. At policy time t the agent observes a proprioception window $p_t \in \mathbb{R}^{d_p}$ (history length 6, see Section C.2) and a multi-ball history tensor $X_t \in \mathbb{R}^{H \times N \times d}$ ($H=4$ object frames, $d=14$: ball position, velocity, orientation, angular velocity, activity flag). Inactive slots are zero-masked. We use H exclusively for the object-history length throughout the main body, and write X for a generic such tensor when no time index is needed. Because the balls are identical, the correct physical equivalence class of a history tensor X is

$$[X]_{G_{\text{frame}}} = \{g \cdot X : g \in G_{\text{frame}}\},$$

and the policy value function should be constant on each orbit. We define the *curriculum-reachable ball count* at training budget B :

$$K_{\max}(E; B) = \max\{k : \text{Succ}_k(E; B) \geq \eta\}, \quad (2)$$

where Succ_k is the success rate on k -ball evaluation episodes and η is the advancement threshold.

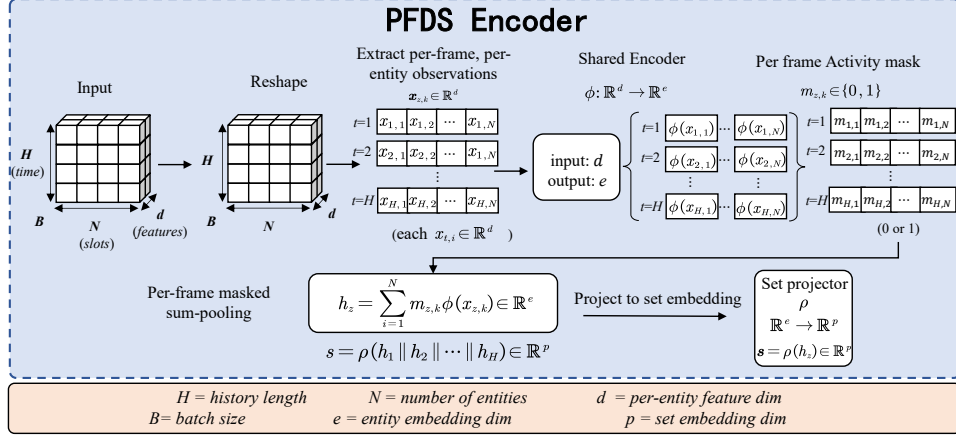


Figure 2: PFDS encoder architecture. Per-object observations $x_{t,i}$ are pooled independently within each history frame t to produce frame embeddings h_t ; these are then concatenated and processed by the readout MLP ρ . Because pooling occurs *within* each frame, the encoder is invariant to independent per-frame permutations (G_{frame} -invariant by Proposition 1).

Evaluation metrics. We define two post-training success metrics evaluated over 100 episodes; the 95% Wilson confidence interval is approximately ± 5 –8 pp at success rates near 0 or 1 and widest ($\approx \pm 10$ pp) near 50%. *No-drop*: the episode completes all 500 steps without any sphere falling off the plate—this is the *primary* task metric, measuring whether the symmetry-aware encoder can maintain multi-sphere transport. *Strict*: additionally requires zero near-edge events throughout the episode (the ball never exits the safe zone), measuring conservative margin performance. Because near-edge events are sensitive to the amount of training received at each curriculum level, the strict metric conflates architectural quality with training exposure; we therefore report both but treat no-drop as the primary measure of encoder capability.

4 Method

4.1 Per-Frame Deep Sets (PFDS)

PFDS decouples *within-frame* set aggregation from *cross-frame* temporal fusion. It modifies standard Deep Sets [10] as

$$h_t = \text{Pool}(\{\phi(x_{t,i})\}_{i \in \mathcal{A}_t}), \quad t = 1, \dots, H, \quad (3)$$

$$z = \rho([h_1; h_2; \dots; h_H]), \quad (4)$$

where $\phi: \mathbb{R}^d \rightarrow \mathbb{R}^e$ is a shared per-element MLP, Pool is a continuous permutation-invariant aggregator on finite multisets (Definition 1; we use masked sum throughout, and the construction also admits mean or max), and ρ is a temporal readout MLP. A slot permutation π_t acts on both the observation tensor and the activity mask, mapping $(\mathcal{A}_t, x_{t,\cdot})$ to $(\pi_t(\mathcal{A}_t), x_{t,\pi_t^{-1}(\cdot)})$, so that h_t depends only on the multiset $\{x_{t,i}\}_{i \in \mathcal{A}_t}$.

Proposition 1 (G_{frame} -invariance of PFDS). f_{PF} is G_{frame} -invariant in the sense of Definition 2: for every $g \in G_{\text{frame}}$ and every X , $f_{\text{PF}}(g \cdot X) = f_{\text{PF}}(X)$.

(Proof in Section A.)

Contrast with DSHC. The standard Deep Sets encoder [10] applied to multi-frame histories forms per-slot tokens $y_i = [x_{1,i}; \dots; x_{H,i}] \in \mathbb{R}^{Hd}$ and computes

$$f_{\text{HC}}(X) = \rho\left(\sum_{i=1}^N \phi_Z(y_i)\right), \quad \phi_Z: \mathbb{R}^{Hd} \rightarrow \mathbb{R}^e. \quad (5)$$

We call this DSHC (Deep Sets, History-Concat). Because ϕ_Z couples frame index t with slot index i , f_{HC} satisfies only G_{diag} invariance, not G_{frame} . PFDS recovers G_{frame} invariance by pooling within each frame *before* temporal concatenation.

Proposition 2 (G_{diag} but not G_{frame} invariance of DSHC). f_{HC} is G_{diag} -invariant. It is, however, not G_{frame} -invariant in general (in the sense of [Definition 2](#)): for any $H \geq 2$ and $N \geq 2$ there exist a continuous feature map ϕ_Z (for instance the flattened outer product $\phi_Z(y) = \text{vec}(yy^\top)$), a continuous readout ρ , an input X , and an element $g \in G_{\text{frame}} \setminus G_{\text{diag}}$ such that $f_{\text{HC}}(g \cdot X) \neq f_{\text{HC}}(X)$.

(Proof in [Section A](#).)

The ratio $|G_{\text{frame}}|/|G_{\text{diag}}| = (N!)^{H-1}$ quantifies the residual representational gap; for $N=5$, $H=4$ this equals $(120)^3 \approx 1.7 \times 10^6$.

Theorem 1 (Universal approximation of PFDS for G_{frame} -invariant functions). Fix the per-frame cardinalities $m_t = |\mathcal{A}_t|$ for $t = 1, \dots, H$ and let $K \subset \mathbb{R}^d$ be a compact box of admissible per-object observations. Let $\Omega = \prod_{t=1}^H K^{m_t}$, and let $G = \prod_{t=1}^H \mathfrak{S}_{m_t}$ act on Ω frame-wise by permuting each K^{m_t} factor. This action coincides with the induced action of G_{frame} on the fixed-cardinality canonical slice $\Omega \hookrightarrow \mathbb{R}^{H \times N \times d}$ (active-slot embedding with the remaining $N - m_t$ slots zero-masked). If $\phi : \mathbb{R}^d \rightarrow \mathbb{R}^e$ and $\rho : \mathbb{R}^{He} \rightarrow \mathbb{R}^a$ are realised by sufficiently wide continuous MLPs and Pool is sum-pooling, then PFDS is dense, under the sup-norm, in the space of continuous G -invariant functions $f : \Omega \rightarrow \mathbb{R}^a$ (equivalently, in the continuous functions on the quotient $\mathcal{X} = \Omega/G$).

(Proof sketch in [Section A](#); the result is a direct corollary of [Deep Sets](#) universality applied frame-wise followed by an MLP readout.)

4.2 Tactile Student Policy (TactSet)

The PFDS teacher uses privileged ball-state observations X_t during training. On the physical robot these are unavailable; only a 16×16 binary contact map is observed. TACTSET bridges this gap by imitating the teacher from a tactile map $\tau_t \in \{0, 1\}^{16 \times 16}$ defined as the Boolean union of active balls' contact footprints. Let $(\bar{x}_{t,i}, \bar{y}_{t,i}, \bar{z}_{t,i})$ denote the centre of ball i at time t expressed in the back-plate frame, and (\bar{x}_s, \bar{y}_s) the planar centre of cell s in the same frame:

$$\tau_{t,s} = \bigvee_{i \in \mathcal{A}_t} \mathbf{1}(|\bar{x}_{t,i} - \bar{x}_s| < r + \delta_x, |\bar{y}_{t,i} - \bar{y}_s| < r + \delta_y, |\bar{z}_{t,i} - (z_{\text{plate}} + r)| < \epsilon_z), \quad (6)$$

where z_{plate} is the height of the plate surface and the z -condition gates contact between the sphere's bottom pole and the plate. Because \vee is symmetric in its arguments, τ_t depends only on the multiset of contact footprints and is a function of $[X_t]_{G_{\text{frame}}}$, semantically aligning the student input with the teacher's observation. We stack tactile maps into a history $\mathcal{T}_t = [\tau_{t-H+1}; \dots; \tau_t] \in \{0, 1\}^{H \times 16 \times 16}$ matching the object-history length H . The student minimises

$$\min_{\theta} \mathbb{E}_{(p_t, X_t, \mathcal{T}_t) \sim \mathcal{D}} \left[\left\| \pi_S^\theta(p_t, \mathcal{T}_t) - \pi_T(p_t, X_t) \right\|_2^2 \right], \quad (7)$$

with DAgger-style online aggregation (behaviour-cloning initialisation followed by 7 rounds of online rollout with PFDS labelling). The student pre-encoder applies a 3×3 2-D CNN to the tactile stack ($H \times 16 \times 16$, 64 channels) followed by a GRU (hidden size 512) that produces a 64-D embedding fed, together with the proprioception embedding, into the policy head (full hyperparameters in [Table 4](#)).

5 Experiments

5.1 Setup

All teacher policies are trained in Isaac Lab [1] with PPO [24] using 4096 parallel environments for 30 000 iterations. Reward, curriculum, and hyperparameters are identical across encoders; only the set-encoding module varies. Full hyperparameters are listed in [Table 3](#).

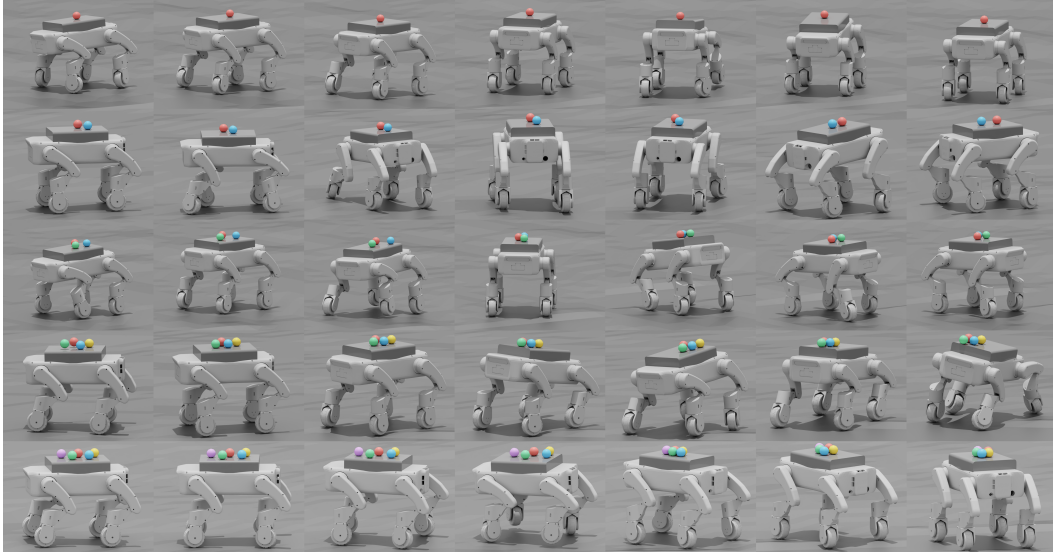


Figure 3: Simulation demonstration of multi-sphere transport with S2M-Trek. Each row shows frames from a representative episode at $k=1$ (top) through $k=5$ (bottom) balls.

Table 1: Teacher encoder comparison under equal PPO budget (30 000 iters). K_{\max} : highest curriculum level reached. “Adv. to k ”: iterations (thousands) to first reach that level; “—” = not reached within budget. Inv.: invariance group. Strict/no-drop: 5-ball success rates (100 trials, 95% Wilson CI $\approx \pm 5$ –8 pp); no-drop is the primary metric (Section 3). †: only G_{frame} encoder reaching $k=5$ without slot-permutation augmentation.

Encoder	Inv.	perm	K_{\max}	Adv. to 3	Adv. to 5	strict	no-drop
FLAT-MLP	G_0	T	≤ 1	—	—	0%	0%
BRANCH-MLP	G_0	T	≤ 2	—	—	0%	2%
DSHC_OFF	G_{diag}	F	≤ 2	—	—	0%	0%
DSHC	G_{diag}	T	5	$\sim 7.4\text{k}$	$\sim 10.9\text{k}$	68%	98%
Set Transformer	G_{diag}	T	5	$\sim 3.6\text{k}$	$\sim 7.7\text{k}$	10%	94%
Set Transformer (PF, ours)	G_{frame}	T	5	$\sim 7.5\text{k}$	$\sim 16.4\text{k}$	54%	100%
PFDS_OFF (ours) [†]	G_{frame}	F	5	$\sim 16.9\text{k}$	$\sim 27.9\text{k}$	41%	98%
PFDS (ours)	G_{frame}	T	5	$\sim 3.9\text{k}$	$\sim 6.3\text{k}$	41%	100%

Encoder baselines. We compare eight architectures spanning three symmetry levels (Table 1), all configured to comparable parameter budgets through matched hidden widths. G_0 (*no invariance*): FLAT-MLP flattens X into a single vector; BRANCH-MLP encodes each slot $X_{:,i}$ with a shared MLP and concatenates the results. G_{diag} (*invariance*): DSHC [10] forms history-concatenated tokens $y_i = [x_{1,i}; \dots; x_{H,i}]$ and applies Deep Sets pooling; Set Transformer [11] replaces the inner network with ISAB/PMA attention on the same tokens. G_{frame} (*invariance (ours)*): PFDS pools within each history frame before temporal readout (Proposition 1). Set Transformer (PF) is the higher-capacity analogue—frame-wise ISAB/PMA attention—but is not used as the distillation teacher because its wall-clock training time is the highest among G_{frame} encoders. PFDS_OFF disables slot randomisation for PFDS, isolating the architectural guarantee from the data-augmentation pathway.

5.2 Main Comparison: Architecture Determines Curriculum Reachability

Figure 5 reports curriculum progression and Figure 4 reports per-encoder success rates. The results form a clear hierarchy consistent with symmetry-group containment: G_0 encoders (FLAT-MLP, BRANCH-MLP) stall at or below $k=2$; G_{diag} encoders (DSHC, Set Transformer) reach $k=5$ only with slot-permutation augmentation, and DSHC_OFF (slot-permutation augmentation off) is blocked below $k=3$; G_{frame} encoders (PFDS, Set Transformer (PF)) advance under both regimes, the architectural guarantee that motivates our construction.

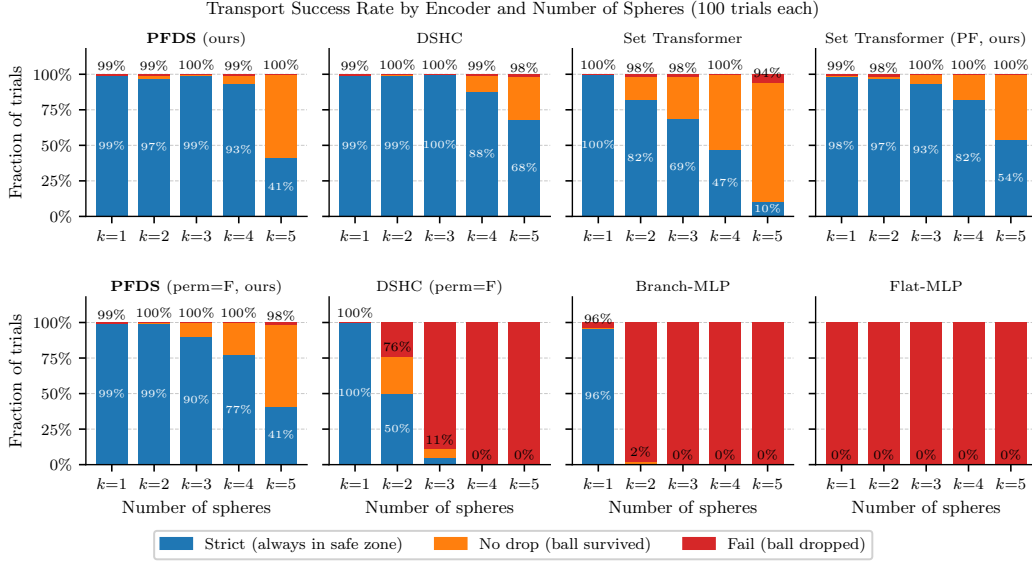


Figure 4: Transport success rates for all eight encoder architectures over 100 trials \times 5 ball counts. Blue: strict (always within safe zone); orange: no-drop (ball survived, may briefly exit); red: fail. G_{frame} -invariant encoders (PFDS, Set Transformer (PF)) achieve 100% no-drop at $k=5$; DSHC with augmentation achieves 98%. G_0 encoders drop to near-zero no-drop beyond $k=1$; DSHC_OFF collapses beyond $k=2$.

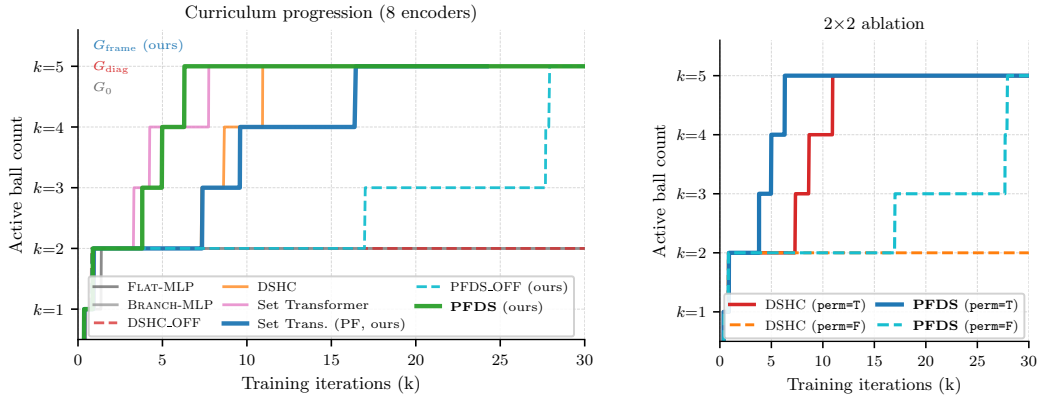


Figure 5: Training dynamics across encoder variants. **Left:** curriculum progression (active ball count vs. iteration) for all eight encoders. G_{frame} architectures (PFDS, Set Transformer (PF)) reach $k=5$ reliably; G_{diag} encoders only with slot-permutation augmentation; G_0 encoders stall at $k \leq 2$. **Right:** 2×2 ablation isolating the architectural and data-augmentation pathways. PFDS reaches $k=5$ with and without augmentation; DSHC fails without it.

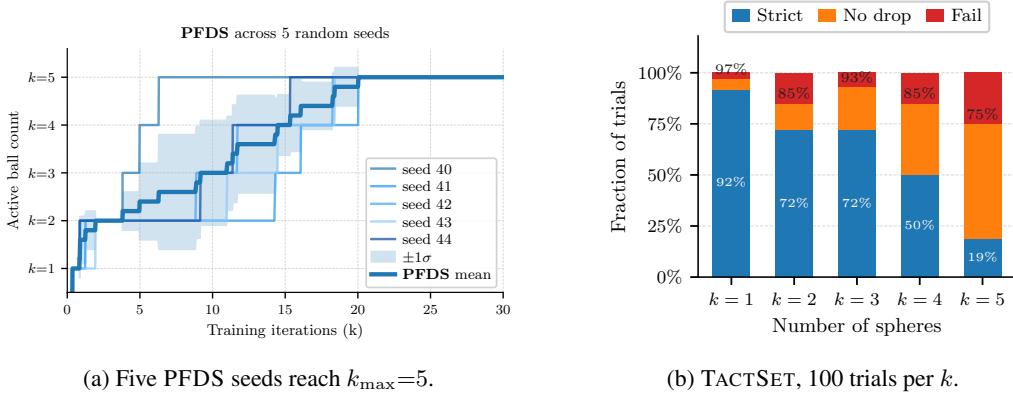
Primary metric (no-drop). PFDS and Set Transformer (PF) achieve 100% no-drop at $k=5$, the highest of any encoder, and PFDS is the fastest to reach the top curriculum level ($\sim 6.3\text{k}$ iters to $k=5$, vs. $\sim 10.9\text{k}$ for DSHC and $\sim 7.7\text{k}$ for Set Transformer). The 2 pp no-drop gap over DSHC is within sampling noise at 100 trials; the substantive differentiator is that PFDS_OFF still attains 98% no-drop without augmentation while DSHC_OFF does not advance past $k=2$ within budget. Robustness with a G_{frame} -invariant architecture is therefore independent of data augmentation, whereas with DSHC it is not.

5.3 2×2 Key Ablation: Two Paths to G_{frame} Robustness

Table 2 and Figure 5 confirm the theoretical prediction in our runs: DSHC reaches $k=5$ only with per-step augmentation ($\pi_t \sim \text{Uniform}(\mathfrak{S}_N)$) and stalls at $k=2$ without it within the 30 000-iteration

Table 2: 2×2 ablation: encoder \times per-step orbit augmentation. “Adv. to 3” is the number of training iterations at which the curriculum first reaches $k \geq 3$; “—” means not reached by 30 000 iterations.

Encoder	permute=True		permute=False	
	K_{\max}	Adv. to 3	K_{\max}	Adv. to 3
DSHC (G_{diag})	5	$\sim 7.4\text{k}$	≤ 2	—
PFDS (G_{frame})	5	$\sim 3.9\text{k}$	5	$\sim 16.9\text{k}$



(a) Five PFDS seeds reach $k_{\max}=5$.

(b) TACTSET, 100 trials per k .

Figure 6: (a) Multi-seed PFDS curriculum progression (mean $\pm 1\sigma$, seeds 40–44). (b) Tactile-student transport success (bar-top: no-drop; inside blue bars: strict).

budget—slot index becomes a spurious proxy for curriculum stage that the G_{diag} encoder cannot ignore. PFDS succeeds in both settings; Section E gives mechanistic details.

5.4 Multi-Seed Robustness and Tactile Distillation

Multi-seed (Figure 6a). Five independent PFDS runs (seeds 40–44, identical PPO hyperparameters) all reach $k_{\max}=5$ within the 30 000-iteration budget; the $\pm 1\sigma$ band reflects variation in convergence timing, not final performance.

Tactile distillation (Figure 6b). We distill the PFDS teacher into TACTSET via the DAGger protocol of Section 4.2 (400 000 BC steps + $7 \times 200\,000$ DAGger steps). The Boolean union contact map is G_{frame} -invariant, placing the student input in the teacher’s equivalence class. Across 100 trials of 500 steps per k , TACTSET attains 97%/92% no-drop/strict at $k=1$ and 75%/19% at $k=5$ (teacher: 100%/41%).

6 Conclusion

We introduced Per-Frame Deep Sets (PFDS), an intrinsically G_{frame} -invariant Deep Sets variant for multi-sphere transport on a wheel-legged robot. Aligning the encoder’s symmetry group with $G_{\text{frame}}=(\mathfrak{S}_N)^H$ —which is $(N!)^{H-1}$ larger than the diagonal group satisfied by history-concatenation encoders—is the key design step. The eight-encoder comparison and the 2×2 ablation together show that G_{frame} -invariant architectures are the only ones robust without slot-permutation augmentation; no-drop differences at $k=5$ among augmented encoders fall within 100-trial sampling noise. PFDS reaches $k_{\max}=5$ across all five seeds, and TACTSET distills the teacher into a purely tactile student that inherits G_{frame} invariance from the Boolean union contact map.

Limitations and future work. All numbers are simulation-only; physical robot deployment is in progress and reported separately. 100-trial Wilson intervals (± 5 –8 pp) support qualitative trends but not fine-grained comparisons. At higher curriculum levels ($k=4$ and $k=5$), the 22.4 cm \times 15.1 cm back plate becomes a binding geometric constraint: five spheres of radius 55 mm require pairwise centre distances of at least 11 cm and cover most of the plate footprint, leaving little spatial margin for ball re-positioning. The strict-rate decrease at $k=5$ therefore reflects, in part, this physical packing

limit rather than a controller deficiency; we plan to enlarge the tactile back plate and revisit higher- k transport in follow-up work. Composed per-type Deep Sets blocks should also extend the principle to heterogeneous object sets.

Acknowledgments

Acknowledgments will be added in the camera-ready version.

References

- [1] M. Mittal et al. Isaac lab: A GPU-accelerated simulation framework for multi-modal robot learning. *arXiv preprint arXiv:2511.04831*, 2025. doi:10.48550/arXiv.2511.04831. URL <https://arxiv.org/abs/2511.04831>.
- [2] J. Hwangbo, J. Lee, A. Dosovitskiy, D. Bellicoso, V. Tsounis, V. Koltun, and M. Hutter. Learning agile and dynamic motor skills for legged robots. *Science Robotics*, 4(26):eaau5872, 2019. doi:10.1126/scirobotics.aau5872.
- [3] N. Rudin, D. Hoeller, P. Reist, and M. Hutter. Learning to walk in minutes using massively parallel deep reinforcement learning. In *Proceedings of the 5th Conference on Robot Learning*, volume 164 of *Proceedings of Machine Learning Research*, pages 91–100. PMLR, 2022. URL <https://proceedings.mlr.press/v164/rudin22a.html>.
- [4] T. Miki, J. Lee, J. Hwangbo, L. Wellhausen, V. Koltun, and M. Hutter. Learning robust perceptive locomotion for quadrupedal robots in the wild. *Science Robotics*, 7(62):eabk2822, 2022. doi:10.1126/scirobotics.abk2822.
- [5] A. Kumar, Z. Fu, D. Pathak, and J. Malik. RMA: Rapid motor adaptation for legged robots. In *Proceedings of Robotics: Science and Systems*, Virtual, July 2021. doi:10.15607/RSS.2021.XVII.011. URL <https://www.roboticsproceedings.org/rss17/p011.html>.
- [6] Y. Ji, G. B. Margolis, and P. Agrawal. DribbleBot: Dynamic legged manipulation in the wild. In *2023 IEEE International Conference on Robotics and Automation (ICRA)*, pages 5155–5162. IEEE, 2023. doi:10.1109/ICRA48891.2023.10160325.
- [7] Z. He, K. Lei, Y. Ze, K. Sreenath, Z. Li, and H. Xu. Learning visual quadrupedal loco-manipulation from demonstrations. In *2024 IEEE/RSJ International Conference on Intelligent Robots and Systems (IROS)*, pages 9102–9109. IEEE, 2024. doi:10.1109/IROS58592.2024.10802742.
- [8] M. Liu, Z. Chen, X. Cheng, Y. Ji, R.-Z. Qiu, R. Yang, and X. Wang. Visual whole-body control for legged loco-manipulation. In *Proceedings of The 8th Conference on Robot Learning*, volume 270 of *Proceedings of Machine Learning Research*, pages 234–257. PMLR, 2025. URL <https://proceedings.mlr.press/v270/liu25b.html>.
- [9] C. Lin, Y. R. Song, B. Huo, M. Yu, Y. Wang, S. Liu, Y. Yang, W. Yu, T. Zhang, J. Tan, Y. Luo, and D. Zhao. Locotouch: Learning dynamic quadrupedal transport with tactile sensing. In *Proceedings of the 9th Conference on Robot Learning*, volume 305 of *Proceedings of Machine Learning Research*, pages 2779–2801. PMLR, 2025. URL <https://proceedings.mlr.press/v305/lin25a.html>.
- [10] M. Zaheer, S. Kottur, S. Ravanbakhsh, B. Poczos, R. Salakhutdinov, and A. Smola. Deep sets. In *Advances in Neural Information Processing Systems*, volume 30, 2017.
- [11] J. Lee, Y. Lee, J. Kim, A. R. Kosiorek, S. Choi, and Y. W. Teh. Set transformer: A framework for attention-based permutation-invariant neural networks. In *Proceedings of the 36th International Conference on Machine Learning*, volume 97 of *Proceedings of Machine Learning Research*, pages 3744–3753. PMLR, 2019.

- [12] C. R. Qi, H. Su, K. Mo, and L. J. Guibas. Pointnet: Deep learning on point sets for 3d classification and segmentation. In *2017 IEEE Conference on Computer Vision and Pattern Recognition (CVPR)*, pages 652–660. IEEE, 2017. doi:10.1109/CVPR.2017.16.
- [13] H. Maron, O. Litany, G. Chechik, and E. Fetaya. On learning sets of symmetric elements. In *Proceedings of the 37th International Conference on Machine Learning*, volume 119 of *Proceedings of Machine Learning Research*, pages 6734–6744. PMLR, 2020.
- [14] E. van der Pol, D. Worrall, H. van Hoof, F. Oliehoek, and M. Welling. Mdp homomorphic networks: Group symmetries in reinforcement learning. In *Advances in Neural Information Processing Systems*, volume 33, pages 4199–4210, 2020.
- [15] E. van der Pol, F. A. Oliehoek, H. van Hoof, and M. Welling. Multi-agent MDP homomorphic networks. In *International Conference on Learning Representations*, 2022. URL <https://openreview.net/forum?id=H7HDG--DJF0>.
- [16] X. Zhu, Y. Qi, Y. Zhu, R. Walters, and R. Platt. EquAct: An SE(3)-equivariant multi-task transformer for 3d robotic manipulation. In *International Conference on Learning Representations*, 2026. URL <https://openreview.net/forum?id=d1wuA8oIH0>.
- [17] T. Hoang, H. Le, P. Becker, V. A. Ngo, and G. Neumann. Geometry-aware RL for manipulation of varying shapes and deformable objects. In *International Conference on Learning Representations*, 2025. URL <https://openreview.net/forum?id=jB0hVc0tsT>.
- [18] J. McClellan, N. Haghani, J. Winder, F. Huang, and P. Tokekar. Boosting sample efficiency and generalization in multi-agent reinforcement learning via equivariance. In *Advances in Neural Information Processing Systems*, volume 37, pages 41132–41156, 2024. URL https://proceedings.neurips.cc/paper_files/paper/2024/hash/4830a9b95a2f63fc4b3fe09abc18f045-Abstract-Conference.html.
- [19] R. S. Dahiya, G. Metta, M. Valle, and G. Sandini. Tactile sensing—from humans to humanoids. *IEEE Transactions on Robotics*, 26(1):1–20, 2010. doi:10.1109/TRO.2009.2033627.
- [20] S. Luo, J. Bimbo, R. Dahiya, and H. Liu. Robot tactile perception of object properties: A review. *Mechatronics*, 48:54–67, 2017. doi:10.1016/j.mechatronics.2017.11.002.
- [21] M. B. Villalonga, A. Rodriguez, B. Lim, E. Valls, and T. Sechopoulos. Tactile object pose estimation from the first touch with geometric contact rendering. In *Proceedings of the 2020 Conference on Robot Learning*, volume 155 of *Proceedings of Machine Learning Research*, pages 1015–1029. PMLR, 2021. URL <https://proceedings.mlr.press/v155/villalonga21a.html>.
- [22] J. Lloyd and N. F. Lepora. Pose-and-shear-based tactile servoing. *The International Journal of Robotics Research*, 43(7):1024–1055, 2024. doi:10.1177/02783649231225811.
- [23] S. Ross, G. Gordon, and D. Bagnell. A reduction of imitation learning and structured prediction to no-regret online learning. In *Proceedings of the Fourteenth International Conference on Artificial Intelligence and Statistics*, pages 627–635. JMLR Workshop and Conference Proceedings, 2011.
- [24] J. Schulman, F. Wolski, P. Dhariwal, A. Radford, and O. Klimov. Proximal policy optimization algorithms. *arXiv preprint arXiv:1707.06347*, 2017.
- [25] K. Hornik, M. Stinchcombe, and H. White. Multilayer feedforward networks are universal approximators. *Neural Networks*, 2(5):359–366, 1989. doi:10.1016/0893-6080(89)90020-8.
- [26] R. T. Rockafellar and S. Uryasev. Optimization of conditional value-at-risk. *Journal of Risk*, 2(3):21–41, 2000. doi:10.21314/JOR.2000.038.

- [27] Y. Bengio, J. Louradour, R. Collobert, and J. Weston. Curriculum learning. In *Proceedings of the 26th Annual International Conference on Machine Learning*, pages 41–48. ACM, 2009. doi:10.1145/1553374.1553380.
- [28] S. Narvekar, B. Peng, M. Leonetti, J. Sinapov, M. E. Taylor, and P. Stone. Curriculum learning for reinforcement learning domains: A framework and survey. *Journal of Machine Learning Research*, 21(181):1–50, 2020. URL <https://jmlr.org/papers/v21/20-212.html>.

A Proof Details

A.1 Preliminaries: Permutation and G_{frame} -Invariance

For completeness we recall the two notions of invariance used throughout the paper.

Definition 1 (Permutation invariance of a multiset aggregator). Let $\mathcal{M}_{\leq N}(\mathbb{R}^e)$ denote the set of finite multisets in \mathbb{R}^e of cardinality at most N . A continuous map $\text{Pool} : \mathcal{M}_{\leq N}(\mathbb{R}^e) \rightarrow \mathbb{R}^e$ is permutation-invariant if its value depends only on its argument as a multiset (with multiplicity), i.e. for any finite indexed family $(z_i)_{i \in \mathcal{A}}$ with $|\mathcal{A}| \leq N$ and any bijection $\sigma : \mathcal{A} \rightarrow \mathcal{A}$,

$$\text{Pool}(\{z_{\sigma(i)}\}_{i \in \mathcal{A}}) = \text{Pool}(\{z_i\}_{i \in \mathcal{A}}).$$

Equivalently, for each cardinality $m \leq N$, the restriction of Pool to multisets of size m corresponds to a symmetric continuous function $(\mathbb{R}^e)^m \rightarrow \mathbb{R}^e$. Standard examples include masked sum, mean, and max.

Definition 2 (G_{frame} -invariance of a function on history tensors). With $G_{\text{frame}} = (\mathfrak{S}_N)^H$ acting on $X \in \mathbb{R}^{H \times N \times d}$ by $(g \cdot X)_{t,i} = x_{t,\pi_t^{-1}(i)}$ for $g = (\pi_1, \dots, \pi_H)$, a function $f : \mathbb{R}^{H \times N \times d} \rightarrow \mathbb{R}^a$ is G_{frame} -invariant if

$$f(g \cdot X) = f(X) \quad \text{for all } X \text{ and all } g \in G_{\text{frame}}.$$

A history tensor X and its G_{frame} -orbit $[X]_{G_{\text{frame}}} = \{g \cdot X : g \in G_{\text{frame}}\}$ are identified under any G_{frame} -invariant f , so f factors through the quotient $\mathbb{R}^{H \times N \times d} / G_{\text{frame}}$.

A.2 Proof of Proposition 1 (PFDS is G_{frame} -Invariant)

Proof. Per (1), under $g = (\pi_1, \dots, \pi_H) \in G_{\text{frame}}$ the new slot i at frame t holds the old value at slot $\pi_t^{-1}(i)$; equivalently, the old slot j moves to $\pi_t(j)$, so the active set transforms as $\mathcal{A}_t \mapsto \pi_t(\mathcal{A}_t)$. Therefore

$$h_t(g \cdot X) = \text{Pool}(\{\phi(x_{t,\pi_t^{-1}(i)})\}_{i \in \pi_t(\mathcal{A}_t)}) = \text{Pool}(\{\phi(x_{t,j})\}_{j \in \mathcal{A}_t}) = h_t(X),$$

where the second equality reindexes the multiset by $j = \pi_t^{-1}(i)$, which traverses \mathcal{A}_t exactly once. The two multisets $\{\phi(x_{t,j})\}_{j \in \mathcal{A}_t}$ are identical, so Pool , being a function on multisets, returns the same value. Hence $z(g \cdot X) = \rho([h_1; \dots; h_H]) = z(X)$. \square

A.3 Proof of Proposition 2 (DSHC is G_{diag} - but not G_{frame} -Invariant)

G_{diag} -invariance. For $g = (\pi, \dots, \pi) \in G_{\text{diag}}$, every frame is permuted by the same π , so each per-slot token transforms as $y_i(g \cdot X) = y_{\pi^{-1}(i)}(X)$. The set $\{y_i\}_{i=1}^N$ is therefore permuted as a multiset, and

$$\sum_{i=1}^N \phi_Z(y_i(g \cdot X)) = \sum_{i=1}^N \phi_Z(y_{\pi^{-1}(i)}(X)) = \sum_{i=1}^N \phi_Z(y_i(X)),$$

so $f_{\text{HC}}(g \cdot X) = f_{\text{HC}}(X)$.

Failure of G_{frame} -invariance ($H=2, N=2$ counterexample). Let $X = \begin{pmatrix} a & b \\ c & d \end{pmatrix}$ with rows indexing time and columns indexing slots, and take $g = (\text{id}, (12)) \in G_{\text{frame}} \setminus G_{\text{diag}}$. Then $(g \cdot X)_{1,:} = (a, b)$

and $(g \cdot X)_{2,:} = (d, c)$, so the DSHC tokens are $y_1^g = (a, d)$, $y_2^g = (b, c)$, whereas $y_1 = (a, c)$, $y_2 = (b, d)$. For the linear feature $\phi_Z = \text{id}$, $\sum_i y_i^g = (a + b, c + d) = \sum_i y_i$: the linear feature is incidentally invariant. For the flattened outer-product feature $\phi_Z(y) = \text{vec}(yy^\top)$, a direct computation gives

$$\sum_i y_i y_i^\top = \begin{pmatrix} a^2 + b^2 & ac + bd \\ ac + bd & c^2 + d^2 \end{pmatrix}, \quad \sum_i y_i^g (y_i^g)^\top = \begin{pmatrix} a^2 + b^2 & ad + bc \\ ad + bc & c^2 + d^2 \end{pmatrix},$$

so the $(1, 2)$ -entry differs by $(ad + bc) - (ac + bd) = (a - b)(d - c)$, which is nonzero whenever $a \neq b$ and $c \neq d$. Choose ρ to project onto the coordinate of $\text{vec}(\cdot)$ holding the $(1, 2)$ -entry. Then $f_{\text{HC}}(g \cdot X) - f_{\text{HC}}(X) = (a - b)(d - c) \neq 0$, exhibiting the required ϕ_Z, ρ, X , and $g \in G_{\text{frame}} \setminus G_{\text{diag}}$. The construction trivially extends to any $H \geq 2, N \geq 2$ by padding additional frames and additional slots with constants. \square

A.4 Proof Sketch of Theorem 1 (Universal Approximation of PFDS)

Let $m_t, K, \Omega, G, \mathcal{X}$ be as in the theorem, and let $n_{\max} = \max_t m_t$. Since each frame has *exactly* m_t active slots, an orbit in Ω/G is identified with a tuple of multisets (S_1, \dots, S_H) with $|S_t| = m_t$ (no cardinality ambiguity arises across frames).

(i) *Per-frame injection by symmetric power sums.* For each fixed m and any compact $K \subset \mathbb{R}^d$, the map

$$\phi_m : \mathbb{R}^d \rightarrow \mathbb{R}^{M_m}, \quad \phi_m(x) = (p_\alpha(x))_{|\alpha| \leq m},$$

collecting all monomials of degree at most m in the d coordinates of x , makes $\Phi_m(S) = \sum_{x \in S} \phi_m(x)$ a continuous injection on multisets of *exactly* cardinality m : the resulting multivariate power-sum symmetric functions determine the elementary multisymmetric polynomials of S via the multisymmetric Newton identities, and these in turn determine S uniquely. (We use that $|S|$ is known at the time of decoding, so the multiset $\{0, \dots, 0\}$ at one cardinality is distinguishable from the same elements at any other cardinality by context.) Taking ϕ to include the components ϕ_m for all $m \in \{m_1, \dots, m_H\}$ (or, equivalently, all $m \leq n_{\max}$) produces a single continuous $\phi : \mathbb{R}^d \rightarrow \mathbb{R}^M$ that is shared across frames, matching the PFDS architecture in (3). Each per-frame embedding $\Phi_t(S_t) = \sum_{x \in S_t} \phi(x)$ is then continuous and injective on $K^{m_t}/\mathfrak{S}_{m_t}$.

(ii) *Joint injection.* Concatenating per-frame embeddings,

$$v(X) = [\Phi_1(X_1); \dots; \Phi_H(X_H)] \in \mathbb{R}^{HM},$$

gives a continuous map $\Omega \rightarrow \mathbb{R}^{HM}$ that factors through \mathcal{X} and is injective on \mathcal{X} , since two orbits agree on v iff their per-frame multisets coincide for every t . Since Ω is compact, so is \mathcal{X} , and a continuous bijection from a compact space to a Hausdorff space (here $v : \mathcal{X} \rightarrow v(\mathcal{X}) \subset \mathbb{R}^{HM}$) is a homeomorphism.

(iii) *Readout approximation.* A continuous G -invariant function $f : \Omega \rightarrow \mathbb{R}^a$ descends to a unique continuous $\tilde{f} : \mathcal{X} \rightarrow \mathbb{R}^a$, which by (ii) corresponds to a continuous $\tilde{f} = \tilde{f} \circ v^{-1} : v(\mathcal{X}) \rightarrow \mathbb{R}^a$. Because $v(\mathcal{X})$ is compact (hence closed) in the normal space \mathbb{R}^{HM} , Tietze's extension theorem (applied coordinate-wise) extends \tilde{f} to a continuous $\hat{f} : \mathbb{R}^{HM} \rightarrow \mathbb{R}^a$. Restricting \hat{f} to a compact neighbourhood of $v(\mathcal{X})$ and applying the universal approximation theorem for multilayer perceptrons [25] yields a continuous $\rho : \mathbb{R}^{HM} \rightarrow \mathbb{R}^a$ such that $\sup_{X \in \Omega} \|\rho(v(X)) - f(X)\| < \varepsilon$ for any prescribed $\varepsilon > 0$. \square

B Hyperparameters

C Environment Specification

C.1 Reward Function

The total reward r_t is the sum of object-balancing terms, locomotion terms, and a penalty term:

$$r_t = r_{\text{obj}} + r_{\text{loco}} + r_{\text{penalty}}. \quad (8)$$

Table 3: PPO hyperparameters shared across all teacher encoder experiments.

Parameter	Value	Note
Parallel environments	4096	Isaac Lab
Total iterations	30 000	
Steps per env per iter	24	
Mini-batches	4	
PPO epochs per iter	5	
Learning rate	3×10^{-4}	Adam
Discount γ	0.99	
GAE λ	0.95	
Clip range ϵ	0.2	
KL target	6×10^{-3}	
Entropy coeff.	0.01	
Value loss coeff.	1.0	
Max grad norm	1.0	
Control frequency	50 Hz	
History length H	4	
Max ball count N	5	

Table 4: DAgger distillation hyperparameters (TACTSET).

Parameter	Value
Rounds	8
BC steps (round 0)	400 000
DAgger steps (rounds 1–7)	200 000 each
Batch size (training)	20 000
Teacher inference batch	2 048
Learning rate	5×10^{-4}
CNN kernel	3×3 , 64 channels
GRU hidden size	512
Tactile input shape	$(H, 16, 16)$
CNN embedding dim	64

Object-balancing rewards. Let $\mathcal{A}_t \subseteq \{1, \dots, N\}$ be the set of active ball indices at time t . For each ball $i \in \mathcal{A}_t$, define the *support margin* $\mu_i \in [0, 1]$ as the minimum normalized distance from ball i 's projected position to the plate boundary (1 = plate center, 0 = edge):

$$r_{\text{margin}} = +3.0 \cdot \frac{1}{|\mathcal{A}_t|} \sum_{i \in \mathcal{A}_t} \mu_i, \quad (9)$$

$$r_{\text{tail}} = +1.25 \cdot \text{CVaR}_{0.4}(\{\mu_i\}_{i \in \mathcal{A}_t}), \quad (10)$$

where $\text{CVaR}_{0.4}$ [26] is the conditional value-at-risk at the 0.4 tail, i.e. the conditional mean of the lowest 40% of margins (a tail-risk reward term incentivising stabilisation of the most precarious ball).

$$r_{\text{edge}} = -15.0 \cdot \frac{1}{|\mathcal{A}_t|} \sum_{i \in \mathcal{A}_t} \mathbf{1}[\mu_i < 0], \quad (11)$$

$$r_{\text{spacing}} = +1.5 \cdot \frac{2}{|\mathcal{A}_t|(|\mathcal{A}_t| - 1)} \sum_{i < j} \min(\|p_i - p_j\|_2, d_{\text{max}}), \quad (12)$$

$$r_{\text{spacing, tail}} = +0.75 \cdot \text{CVaR}_{0.4}(\{\|p_i - p_j\|_2\}_{i < j}), \quad (13)$$

$$r_{\text{dangerous}} = -20.0 \cdot \mathbf{1}[\min_{i \in \mathcal{A}_t} \mu_i < \mu_{\text{thresh}}], \quad (14)$$

where $p_i \in \mathbb{R}^2$ is the ball's projected position on the plate, d_{max} is a clipping radius, and μ_{thresh} is the dangerous-state threshold (set per curriculum level).

Velocity-related penalties.

$$r_{\text{vel},xy} = -0.05 \cdot \frac{1}{|\mathcal{A}_t|} \sum_{i \in \mathcal{A}_t} \|v_i^{xy}\|_2^2, \quad (15)$$

$$r_{\text{vel},z} = -0.25 \cdot \frac{1}{|\mathcal{A}_t|} \sum_{i \in \mathcal{A}_t} |v_i^z|, \quad (16)$$

where v_i^{xy} and v_i^z are the ball’s horizontal and vertical velocity in the robot frame.

Locomotion rewards (from base locomotion policy).

$$r_{\text{track},v} = +1.5 \cdot \exp(-\|\hat{v}^{xy} - v_{\text{cmd}}^{xy}\|_2^2/0.25), \quad (17)$$

$$r_{\text{track},\omega} = +1.25 \cdot \exp(-|\hat{\omega}_z - \omega_{z,\text{cmd}}|^2/0.25), \quad (18)$$

$$r_{\text{height}} = -1.0 \cdot (h - h_{\text{ref}})^2, \quad (19)$$

$$r_{\text{roll,pitch}} = -1.25 \cdot \|\theta_{\text{rp}}\|_2^2, \quad (20)$$

where \hat{v}^{xy} and $\hat{\omega}_z$ are the robot’s base velocity, v_{cmd}^{xy} and $\omega_{z,\text{cmd}}$ are the commanded velocities, h is the base height, h_{ref} is the target height, and θ_{rp} are the roll and pitch angles.

C.2 Observation Space

The teacher policy receives the following observations at each timestep:

Proprioception (history length $H_{\text{prop}} = 6$, distinct from the object-history length $H = 4$).

- Base angular velocity $\omega_b \in \mathbb{R}^3$
- Projected gravity vector $g_b \in \mathbb{R}^3$
- Velocity command $[v_x, v_y, \omega_z] \in \mathbb{R}^3$
- Joint positions $q \in \mathbb{R}^{12}$ (relative to default)
- Joint velocities $\dot{q} \in \mathbb{R}^{12}$
- Previous action $a_{t-1} \in \mathbb{R}^{12}$
- Robot base height $h \in \mathbb{R}^1$

Total proprioception dimension: $43 \times H_{\text{prop}} = 258$.

Multi-ball state (object-history length $H = 4$, per-ball feature dim $d = 14$). For each active ball $i \in \mathcal{A}_t$:

- Relative position $\Delta p_i \in \mathbb{R}^3$ (ball position minus robot base, in robot frame; scale 1.0)
- Relative linear velocity $\Delta v_i \in \mathbb{R}^3$ (scale 0.5)
- Relative orientation as quaternion $q_i \in \mathbb{R}^4$ (scale 1.0)
- Relative angular velocity $\omega_i \in \mathbb{R}^3$ (scale 0.25)
- Activity flag $a_i \in \{0, 1\}$ (scale 1.0)

Inactive slots are zero-masked. Observation noise (uniform): position ± 0.01 m, velocity ± 0.2 m/s, orientation ± 0.05 (Euler-angle equivalent), angular velocity ± 0.2 rad/s. Ball state is observable only when the ball is in contact with the robot surface (contact detection threshold $\approx 10^{-8}$ N); otherwise the observation is zero.

The critic (teacher) additionally receives the denoised version of the above (no observation noise added).

C.3 Termination Conditions

An episode terminates (non-timeout) when any of the following occurs:

1. **Ball falls below robot base:** any active ball’s z -position drops below the robot base z -position, $\exists i \in \mathcal{A}_t : p_{i,z} < p_{\text{Robot},z}$.
2. **Robot falls:** the projected gravity vector indicates a roll angle $|\arcsin(g_{b,y})| > 90^\circ$.
3. **Base height too low:** the robot base height falls below the minimum standing height threshold.

Note: the `base_contact` termination (body contact with the ground) is disabled for the multi-sphere task to prevent false positives from the tactile plate surface.

D Curriculum Design

Curriculum learning [27, 28] progresses the agent from easy to hard task instances. In our setting the difficulty axis is the active ball count k .

D.1 Promotion Criteria

The multi-ball curriculum promotes from k to $k + 1$ active balls when a rolling window of recent episodes satisfies *all six* of the following conditions simultaneously:

1. **Episode-length ratio** ≥ 0.85 : the mean episode length divided by the maximum episode length exceeds 85%, indicating the agent consistently survives to episode end.
2. **Support margin** $\geq \mu_k^*$: mean minimum support margin across active balls exceeds the level threshold.
3. **Dangerous fraction** $\leq f_{d,k}^*$: the fraction of timesteps with any ball in a dangerous state (near edge) is below the level threshold.
4. **Edge-overflow fraction** $\leq f_{e,k}^*$: the fraction of timesteps with any ball outside the plate boundary is below the level threshold.
5. **Linear velocity tracking error** $\leq \epsilon_{v,k}^*$: mean $\|\hat{v}^{xy} - v_{\text{cmd}}^{xy}\|_2$ is below threshold.
6. **Angular velocity tracking error** $\leq \epsilon_{\omega,k}^*$: mean $|\hat{\omega}_z - \omega_{z,\text{cmd}}|$ is below threshold.

All conditions must hold simultaneously for `required_successes = 1` consecutive evaluation windows, with `min_stage_episodes = 2048` and `min_steps_per_level = 3200`.

D.2 Per-Level Promotion Thresholds

Table 5: Per-level curriculum promotion thresholds ($k \rightarrow k + 1$). “Support margin” μ^* is the normalized minimum distance from plate boundary. “Dangerous frac.” f_d^* and “Edge frac.” f_e^* are allowed fractions of unsafe timesteps. “Vel. err.” ϵ_v^* and “Yaw err.” ϵ_ω^* are maximum allowed tracking errors.

Level ($k \rightarrow k + 1$)	μ^*	f_d^*	f_e^*	ϵ_v^*	ϵ_ω^*
1 \rightarrow 2	0.30	0.20	0.02	0.30	0.40
2 \rightarrow 3	0.25	0.25	0.03	0.35	0.45
3 \rightarrow 4	0.20	0.30	0.04	0.40	0.50
4 \rightarrow 5	0.15	0.35	0.05	0.45	0.55

The thresholds are relaxed progressively at higher levels to account for the increased difficulty of balancing more balls simultaneously.

E Discussion

Architectural vs. augmentation guarantees. In our runs the failure of `DSHC_OFF` behaves as a budget-limited barrier rather than a convergence delay: slot identity becomes a deterministic proxy for curriculum stage and blocks promotion beyond $k=2$ for the full 30 000-iteration budget. `PFDS` avoids this by construction; without augmentation it advances to $k=5$ but is slower to reach $k \geq 3$

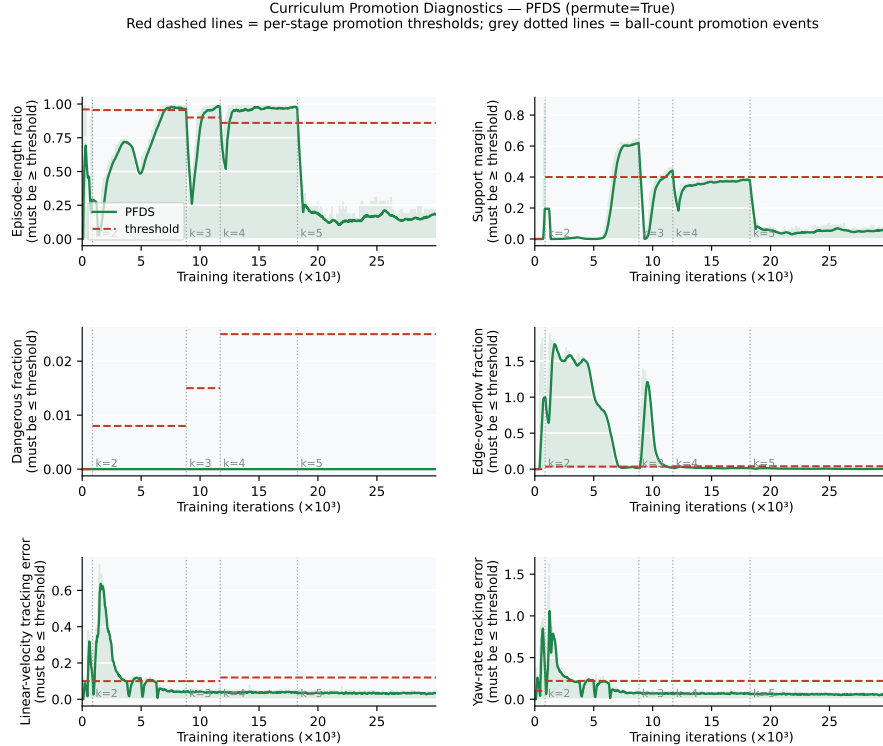


Figure 7: Curriculum promotion-criterion traces for a representative PFDS training run. All six promotion conditions are shown: episode-length ratio, support margin, dangerous-state fraction, edge-overflow fraction, linear-velocity tracking error, and yaw-rate tracking error. Red dashed lines are per-stage promotion thresholds; grey dotted lines mark the iterations at which the curriculum advances to the next level. All six conditions must simultaneously meet threshold for promotion.

($\sim 16.9\text{k}$ vs. $\sim 3.9\text{k}$ iterations, Table 2). Whether longer training or different seeds would eventually unblock DSHC_OFF is left to future work.

Curriculum-dynamics mechanism of DSHC failure. Beyond the symmetry-group argument, the failure has a concrete curriculum-dynamics signature. When slot-permutation augmentation is disabled, slot index i is consistently occupied by ball i across an episode; because the curriculum activates balls sequentially, the slot index becomes a deterministic proxy for the current curriculum stage. The policy keys on slot identity rather than physical state, and fails to satisfy the *conjunction* of promotion criteria at $k=2$: the episode-length ratio remains high (the agent does not fail outright) but the support margin never reaches the promotion threshold. PFDS is immune by construction, since its per-frame pooling discards slot-identity information. Figure 8 reports the resulting traces in the runs we observed.

Sample-efficiency cost of disabling augmentation. Without slot-permutation augmentation, the training distribution samples only the identity element of G_{frame} at each step, reducing effective distributional diversity. Since PFDS is G_{frame} -invariant by construction, this does not prevent convergence but does increase the number of iterations required to cover the state space (Table 2: $\sim 16.9\text{k}$ vs. $\sim 3.9\text{k}$ iterations to $k \geq 3$).

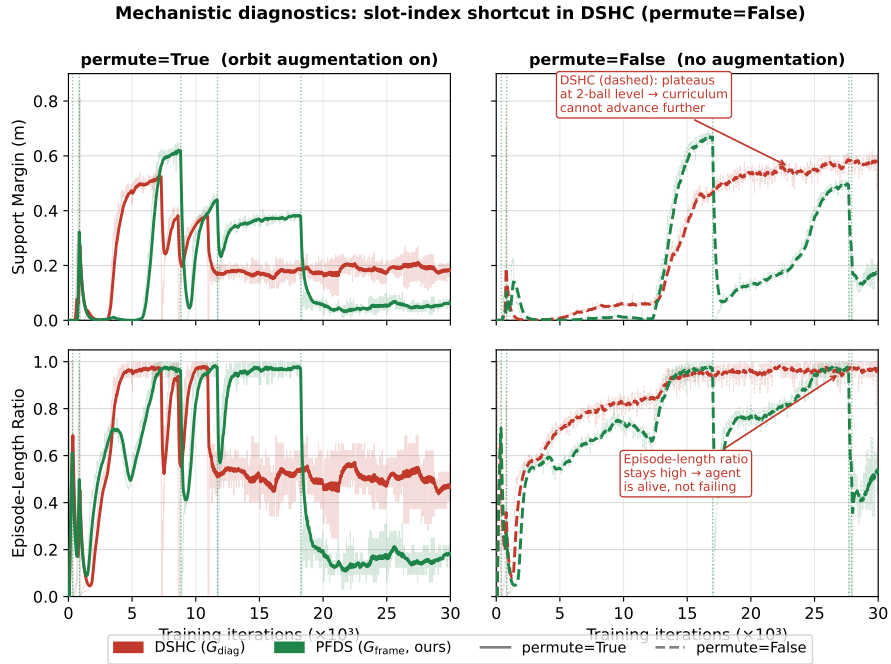


Figure 8: Curriculum-progress diagnostic for the slot-index shortcut. Rows show two promotion-related signals (top: support margin; bottom: episode-length ratio). Columns compare slot-permutation augmentation on (left) and off (right). DSHC (dashed) and PFDS (solid) are overlaid. Under augmentation-off, DSHC_OFF keeps the episode-length ratio high but cannot push the support margin to its promotion threshold, so the curriculum stalls at $k=2$; PFDS_OFF reaches both thresholds and advances. Under augmentation-on, both encoders meet the conjunction of promotion criteria.